Entanglement and co-tunneling of two equivalent protons in hydrogen bond pairs

Zorka Smedarchina, Willem Siebrand, and Antonio Fernández-Ramos

Citation: The Journal of Chemical Physics **148**, 102307 (2018); doi: 10.1063/1.5000681
View online: https://doi.org/10.1063/1.5000681
View Table of Contents: http://aip.scitation.org/toc/jcp/148/10
Published by the American Institute of Physics

Entanglement and co-tunneling of two equivalent protons in hydrogen bond pairs

Zorka Smedarchina,[1,2] Willem Siebrand,[2] and Antonio Fernández-Ramos[1,a)]
[1]*Centro Singular de Investigación en Química Biolóxica e Materiais Moleculares (CIQUS), e Departamento de Química Física, Universidade de Santiago de Compostela, 15782 Santiago de Compostela, Spain*
[2]*National Research Council of Canada, Ottawa, Ontario K1A 0R6 Canada*

(Received 17 May 2017; accepted 17 August 2017; published online 11 September 2017)

A theoretical study is reported of a system of two identical symmetric hydrogen bonds, weakly coupled such that the two mobile protons can move either separately (stepwise) or together (concerted). It is modeled by two equivalent quartic potentials interacting through dipolar and quadrupolar coupling terms. The tunneling Hamiltonian has two imaginary modes (reaction coordinates) and a potential with a single maximum that may turn into a saddle-point of second order and two sets of (inequivalent) minima. Diagonalization is achieved via a modified Jacobi-Davidson algorithm. From this Hamiltonian the mechanism of proton transfer is derived. To find out whether the two protons move stepwise or concerted, a new tool is introduced, based on the distribution of the probability flux in the dividing plane of the transfer mode. While stepwise transfer dominates for very weak coupling, it is found that concerted transfer (co-tunneling) always occurs, even when the coupling vanishes since the symmetry of the Hamiltonian imposes permanent entanglement on the motions of the two protons. We quantify this entanglement and show that, for a wide range of parameters of interest, the lowest pair of states of the Hamiltonian represents a perfect example of highly entangled quantum states in continuous variables. The method is applied to the molecule porphycene for which the observed tunneling splitting is calculated in satisfactory agreement with experiment, and the mechanism of double-proton tunneling is found to be predominantly concerted. We show that, under normal conditions, when they are in the ground state, the two porphycene protons are highly entangled, which may have interesting applications. The treatment also identifies the conditions under which such a system can be handled by conventional one-instanton techniques. *Published by AIP Publishing.* [http://dx.doi.org/10.1063/1.5000681]

I. INTRODUCTION

Many processes in physics, chemistry, and biology involve tunneling of (quasi)particles between two equivalent configurations separated by a barrier. If the particles occur in pairs, the question arises whether these particles tunnel concertedly (co-tunneling) or stepwise. It seems clear that strong interaction between the particles will favor co-tunneling, but even if there is no interaction, quantum mechanics imposes a degree of dependence if the particles are identical and their configurations are equivalent, as has been well recognized for electrons, spins, and qubits (see Ref. 1 and references therein). It is the purpose of this paper to introduce and study a new example of this type, namely, two protons in equivalent symmetric hydrogen bonds. Well-known examples are carboxylic acid dimers[2–4] and porphycenes[5,6] (see Fig. 1), where the hydrogen bonds occur in pairs. Since hydrogen bonds are polar, they will interact, which will support co-tunneling of the protons. For instance, in the formic acid dimer, where the O–H hydrogen bonds show strong polarity, the interaction will be very strong and we know that the two protons tunnel as a single particle since the tunneling potential shows an ordinary (first-order) transition state and the observed tunneling splitting is very small, as expected for double-proton transfer. By contrast, in porphycene, the N–H hydrogen bonds are much weaker, leading to a greatly reduced dipole interaction; correspondingly, the tunneling barrier is a second-order saddle point and the large tunneling splitting is close to what is expected for single-proton transfer although it is not immediately clear whether it can be interpreted that way. Quantum-chemical calculations show that in porphycene the second-order saddle point connects not only the two equilibrium configurations along one tunneling coordinate but also two equivalent secondary minima along another so that there is an alternative tunneling path, involving the secondary minima. It is not evident, however, which path is preferred.

In this paper, we focus on double-proton transfer in molecules and complexes with two equivalent hydrogen bonds in which the potential energy surface shows four pair-wise equivalent minima. Although not many of such systems are known to date, they are of fundamental significance since they introduce the problem of proton tunneling through two-dimensional (2D) barriers and allow investigation of the range of cooperativity of proton motion in systems with coupled hydrogen bonds. Thus far these systems, in which the coupling is weak enough to allow both separate and concerted

a)Author to whom correspondence should be addressed: qf.ramos@usc.es

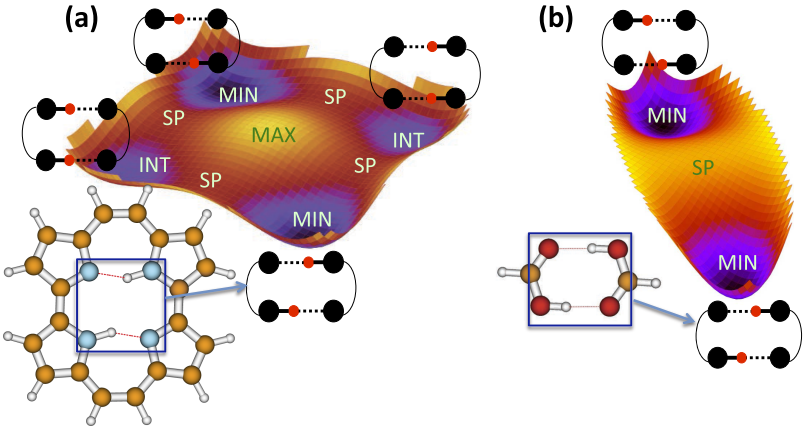

FIG. 1. Two potential energy surfaces for double-proton transfer represented by two equivalent symmetric hydrogen bonds, (a) porphycene and (b) formic acid dimer [colors in the hydrogen-bond pairs shown in the blue boxes: blue (nitrogen), brown (carbon), white (hydrogen), and red (oxygen)].

proton transfer, have not been systematically investigated. Such an investigation requires the inclusion of proton-proton correlation in the dynamics and thus calls for a full quantum treatment since alternative instanton techniques would give rise to interference effects if more than one instanton is present. The method we will adopt is based on direct diagonalization of an imaginary-mode Hamiltonian of a type we introduced earlier for 1D tunneling.[7–9] A fundamental assumption is that this Hamiltonian can be written as the sum of two equivalent single-proton Hamiltonians plus a coupling. In these single-proton Hamiltonians, the proton moves in a symmetric double-minimum potential. To show the full extent of the cooperativity, we choose a symmetric arrangement in which the two single-proton Hamiltonians are identical and coupled by terms up to the fourth order in the tunneling coordinates, such that the overall symmetry corresponds to the point group D_{2h}. This Hamiltonian, derived in Sec. II, is a generalization of the Hamiltonian previously handled by instanton techniques,[10] which was restricted to dipole coupling. In its previous version, it has been applied by us[10] and others[11–13] to a number of such double-proton transfer processes with various arrangements of the two hydrogen bonds. Investigations of alternative 2D Hamiltonians with more than one transition state have been reported in the literature,[14–16] but these were limited to potentials with only one set of minima and thus without a stable intermediate; moreover, they do not (generally) decompose into two 1D Hamiltonians and a coupling, and thus fail to meet the fundamental assumption formulated above, expected to be required for application to a pair of weakly coupled hydrogen bonds. The only exception is the model based on diabatic states developed recently by McKenzie,[17] which has some similarity to our Hamiltonian of Ref. 10.

In Sec. III, the Hamiltonian is diagonalized, first in a simplified form so as to allow an analytical solution to show the symmetry properties, and thereafter numerically with a modified Jacobi-Davidson algorithm for sparse matrices.[18] The resulting eigenvalues yield tunneling splittings and the eigenfunctions contain information on the nature of the proton transfer mechanism responsible for these splittings. The eigenfunctions also reveal the degree of entanglement of the two protons (i.e., their deviation from separability), manifested in specific localization in the 2D space of continuous variables (CV) defined by the proton coordinates. To turn the information contained in the eigenfunctions into an explicit form, we introduce in Sec. III a new entanglement measure in CV, termed "confinement" and show that the lowest pair of states of the Hamiltonian is highly entangled for a wide range of parameters of interest. To obtain information on the proton transfer mechanism, we introduce in Sec. IV a new method, which consists of calculating the probability flux between the eigenstates involved in the transfer. The distribution of this flux in the dividing plane answers the original question: when and to what extent can the cooperative tunneling be separated into two distinct regimes, whereby the two particles move concertedly or stepwise. Specifically, the flux distribution reveals the favored tunneling pathways of two protons in coupled hydrogen bonds and allows a formal distinction between concerted and stepwise tunneling processes and their dependence on the potential. After testing the method in Sec. V by applying it to double-proton transfer in a real system (porphycene), we use it in Sec. VI to assess the range of validity of conventional one-instanton techniques previously applied to double-proton transfer.[3,19]

II. THE MODEL HAMILTONIAN

We consider a model of two identical particles of mass m moving in identical symmetric double-minimum potentials, denoted by $U(x_{1,2})$ in a symmetric arrangement corresponding to the point group D_{2h}. We rewrite their simplest form, $U(x) = -ax^2 + bx^4$, in terms of the stationary states $U(0) = 1/2$ and $U(\pm 1) = 0$, which define, respectively, the height and the halfwidth of the central barrier, to be denoted by U_0 and Δx; in dimensionless units, and the 1D potential then reads $U(x) = (1/2)(1 - x^2)^2$. The lowest-order symmetry-allowed couplings between the two particles are proportional to x_1x_2 (dipole coupling): $x_1^2x_2^2$ (quadrupole coupling) and $x_1x_2^3 + x_2x_1^3$ (dipole-octupole coupling). The resulting 2D model Hamiltonian contains and is limited to all symmetry-allowed terms up to the fourth power of x; scaling energy again by $2U_0$ and coordinates by Δx, it takes the following dimensionless form:

$$H_{2D}(x_1, x_2) = -\frac{1}{2}g^2\left(\frac{\partial^2}{\partial x_1^2} + \frac{\partial^2}{\partial x_2^2}\right) + \sum_{i=1,2} U_i(x_i) - 2Gx_1x_2 - Dx_1^2x_2^2 - C(x_1^3x_2 + x_2^3x_1), \quad (1)$$

where $g = \hbar/\Delta x\sqrt{2mU_0}$ is the dimensionless equivalent of $\hbar$, and G, D, and C are the corresponding coupling constants. Although formally allowed by symmetry, the last interaction term is negligible in realistic systems and will be omitted from further consideration. We take U_1 and U_2 to be antiparallel in the sense that the two equilibrium configurations correspond to $x_1 = x_2 = \pm 1$ and the two secondary minima, if they exist, at $x_1 = -x_2 = \pm 1$ for $G > 0$, i.e., repulsive interaction, as in our case. Changing the sign of G changes only the relative sign of x_1 and x_2 at the minima and thus does not affect the generality of the treatment. There is no restriction on the sign of D, but there is one on its magnitude for we assume that the multipole expansion converges uniformly, i.e., that the quadrupole coupling, as formulated, is weaker than the dipole coupling: $|D| < 2G$. We showed in Ref. 3 that this Hamiltonian (without the quartic coupling) represents two coupled identical hydrogen bonds, where $U(x_{1,2})$ are the double-minimum potentials along the proton coordinates.

To relate the individual coordinates $x_{1,2}$ to the symmetry of the potential, we transform Eq. (1) to collective coordinates

$$x_s = (x_1 + x_2)/2, \quad x_a = (x_1 - x_2)/2, \quad m_s = 2m. \tag{2}$$

This leads to the following form of the Hamiltonian, which again consists of two coupled quartic potentials, and for comparison, we list also the potential of uncoupled particles V^0_{2D}:

$$\begin{aligned} H_{2D}(x_s, x_a) &= -\frac{1}{2}g_s^2\left(\frac{\partial^2}{\partial x_s^2} + \frac{\partial^2}{\partial x_a^2}\right) + V_{2D}; \\ V_{2D} &= (1-D)[(x_s^2 - \Delta x_s^2)^2 + (x_a^2 - \Delta x_a^2)^2 + 2Rx_s^2x_a^2]; \\ V^0_{2D} &= (x_s^2 - 1)^2 + (x_a^2 - 1)^2 + 6x_s^2x_a^2, \end{aligned} \tag{3}$$

where $g_s = \hbar/\Delta x\sqrt{2m_sU_0}$, $\Delta x_s = \sqrt{(1+G)/(1-D)}$, $\Delta x_a = \sqrt{(1-G)/(1-D)}$, and $R = (3+D)/(1-D)$. While the quadrupole coupling does not affect the symmetry of the potential, it does affect its shape and the strength of coupling between x_s and x_a: for $D > 0$, it makes the potential wider and flatter, and increases the coupling constant R; for $D < 0$, it makes the potential narrower and higher but decreases R. The potential in Eqs. (1) and (3) is defined by four parameters: $U_0, \Delta x, G$, and D. In the form of Eq. (3), it can be directly related to the quantum-chemically calculated potential of a given molecule or complex. Methods to extract the model parameters from the calculated potential are discussed in Sec. V and in the Appendix.

The potential in Eqs. (1) and (3) has up to nine stationary configurations, of up to four different types.[3] The most symmetric configuration, denoted by MAX, has the protons in the center of its bonds. Having the highest symmetry and also, since the interaction is repulsive, the highest energy, it serves as a barrier between the two most stable configurations with the protons in the *trans* position ($x_1 = x_2 = \pm 1$), denoted by MIN. MAX also serves as a barrier between the corresponding *cis* configurations ($x_1 = -x_2 = \pm 1$), denoted by INT (for intermediate), if these are stable, in which case MAX assumes the form of an SP2 if other degrees of freedom are added. The fourth stationary configuration, if it exists, is a first-order saddle point (SP), which serves as a transition state between *cis* and *trans* configurations. Figure 1(a) illustrates the potential-energy landscape with a stable INT, which is considered here. If the stable intermediate collapses into a SP, the potential supports a single set of minima, connected through two tunneling pathways: one through the SP2, and the other through the SP; such scenarios have been analyzed in the literature.[14–16]

The stationary points and the corresponding frequencies $\omega_{s,a}$ are defined with respect to the collective coordinates $x_{s,a}$, which represent the modes with imaginary frequencies at the SP2; in the adopted units, they are scaled by a "scaling frequency" Ω defined as $\Omega = \sqrt{2U_0/m_0}/\Delta x$, where m_0 is the proton mass. For our basic assumptions $G > 0$ and $|D| < 2G$, the condition for global minima is $D < 1$; then, if $0 < G < 1$, MAX will be an SP2; if $G > 1$, it turns into a SP. Within the limits where MAX is an SP2, a pair of stable intermediates INT will always exist if $G < 1/4$, and if $D > 2G - 1$ for larger G; if $D < 2G - 1$, the INT collapses into a SP. These regimes are depicted in Fig. 2, where we consider only systems with an SP2, i.e., those with $G < 1$. The red color represents systems with INT and the green color represents systems with INT replaced by an SP; the latter were studied in Refs. 14–16. Areas not within the cone of the solid lines are outside our convergence limit $|D| < 2G$; white areas represent unphysical combinations.

Since the green area represents systems with a single set of minima, it can be treated by instanton techniques in a straightforward way; however, as there are two saddle points, two instantons are possible: a 1D instanton that connects the minima through the SP2, termed here "concerted" instanton, and a 2D instanton that connects them through the SP. The green area corresponds to a tunneling regime governed by the concerted instanton, as we show elsewhere.[20] The symbols represent alternative tunneling regimes, but are outside the convergence cone and therefore of no interest to us. The problem of

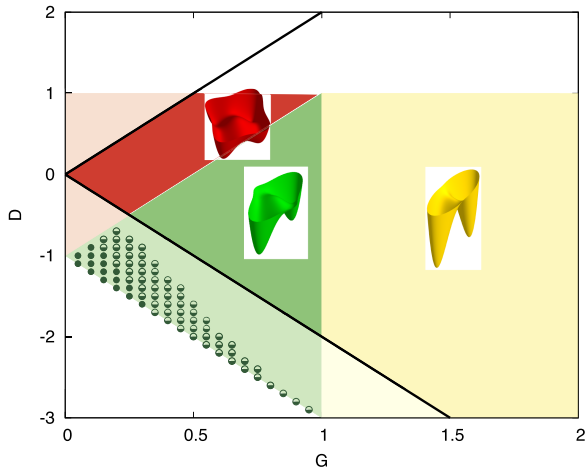

FIG. 2. Coupling regimes supported by the model potential represented by Eq. (1). The colored areas are associated with potential energy surfaces of the same color. The solid lines represent the limiting condition $|D| < 2G$. Red color corresponds to systems with a stable intermediate (INT), whereas green and yellow colors correspond to systems without INT; for the other symbols, which are outside the range of parameter values of our model, see text.

two-proton tunneling in realistic systems of this type can thus be solved by standard instanton techniques based on the concerted instanton; in Sec. VI, we report such calculations for the 2D Hamiltonians (1,3). We thus consider the problem solved for potentials of this type.

Here we focus on systems with INT within our imposed parameter limits, represented by the red area inside the cone. In this case, the application of instanton techniques is more complicated since the two sets of minima support two distinct families of instantons, which will be generally subject to interference. For that reason we avoid the instanton approach and adopt a full quantum treatment. We return to this problem in Sec. VI, where we compare the quantum results with those obtained from the one-instanton approximation based on the concerted instanton.

A complete solution of the multidimensional vibrational Hamiltonian of a complex molecule with two tunneling coordinates far exceeds our present computational capabilities. One of the closest approaches in this direction involves the study of the vibration-rotation tunneling spectrum of the $(NNO)_2$ dimer.[21] In that work, the rovibrational Schrödinger equation is solved using the Lanczos algorithm and an uncoupled product basis set. Another interesting work, but restricted to a single tunneling coordinate, is the study of malonaldehyde, the benchmark molecule for 1D tunneling, by Hammer and Manthe.[22] These authors generated eigenvalues, which, for energies up to about 1400 cm^{-1}, show very good agreement with measured tunneling splittings; at higher energies, they encountered convergence problems. While this calculation provides an important landmark, it turned out that the results could not be easily interpreted in terms that allow generalization to other molecules. The complex problem of analyzing the splittings in terms of the multimode wave functions was never attempted; the qualitative interpretation we provided later[23] is based on general principles and on symmetry.

III. SYMMETRY AND ENTANGLEMENT

A. An approximate solution

Before discussing numerical diagonalization of the Hamiltonian (1) or (3), we consider an approximate analytical diagonalization for the zero-point states only. It will apply if levels involving excitation of high-frequency vibrations (such as OH-stretch modes) are well separated from the zero-point levels; this will generally be the case if the coupling is very weak ($G << 0.5$) and quadrupole coupling can be neglected, i.e., $D = 0$.

In this approximation, the basis set is reduced to the four products $\phi_1^{\pm}\phi_2^{\pm}$, where $\phi(x)^{\pm}$ are the two zero-point eigenfunction for the 1D potential $U(x)$ with (dimensionless) eigenvalues $\epsilon^{\pm} = \frac{1}{2}(\omega_0 \mp \Delta_0)$; the subscripts 1 and 2 refer to the two protons and the superscripts + and − refer to wave functions with an even and odd number of nodes, respectively. Alternatively, one can form eigenfunctions of the proton pair localized in the *trans* (T) and *cis* (C) configuration, respectively,

$$\psi_s^T = (1/\sqrt{2})(\phi_1^+\phi_2^+ + \phi_1^-\phi_2^-), \quad \psi_a^T = (1/\sqrt{2})(\phi_1^+\phi_2^- + \phi_1^-\phi_2^+),$$
$$\psi_s^C = (1/\sqrt{2})(\phi_1^+\phi_2^+ - \phi_1^-\phi_2^-), \quad \psi_a^C = (1/\sqrt{2})(\phi_1^+\phi_2^- - \phi_1^-\phi_2^+), \tag{4}$$

where the subscripts s and a (not in *italics*) refer to symmetric and antisymmetric functions. The 2D eigenfunctions are denoted by $\Phi^{\pm}$ with subscripts I, II, III, and IV in ascending order of energy corresponding to eigenvalues E_I, E_{II}, E_{III}, and E_{IV}. If there is no coupling ($G = 0$), the eigenvalues of the symmetric eigenstates Φ_I and Φ_{IV} are separated by $2\Delta_0$, i.e., twice the zero-point splitting of the 1D potential $U(x)$. The degenerate antisymmetric states Φ_{II} and Φ_{III} are located halfway between the two symmetric eigenstates. Introduction of dipolar coupling splits them into components whose properties are determined by symmetry; for $G > 0$, the *trans* component has the lower energy.

Since the 2D Hamiltonian (1,3) is of D_{2h} symmetry, its eigenvectors (wave functions) are of a_g, b_{3g}, and b_{2u} type; analytical diagonalization of the 4×4 matrix of Hamiltonian (1) with $D = 0$ then yields

$$\begin{aligned}
\Phi_I^+(a_g) &= C_+\phi_1^+\phi_2^+ + C_-\phi_1^-\phi_2^- = C_T\psi_s^T + C_C\psi_s^C, & E_I &= \omega_0 - \Delta_0\sqrt{1+\kappa^2},\\
\Phi_{II}^-(b_{3g}) &= (1/\sqrt{2})(\phi_1^+\phi_2^- + \phi_1^-\phi_2^+) = \psi_a^T, & E_{II} &= \omega_0 - \kappa\Delta_0,\\
\Phi_{III}^-(b_{2u}) &= (1/\sqrt{2})(\phi_1^+\phi_2^- - \phi_1^-\phi_2^+) = \psi_a^C, & E_{III} &= \omega_0 + \kappa\Delta_0,\\
\Phi_{IV}^+(a_g) &= -C_-\phi_1^+\phi_2^+ + C_+\phi_1^-\phi_2^- = -C_T\psi_s^T + C_C\psi_s^C, & E_{IV} &= \omega_0 + \Delta_0\sqrt{1+\kappa^2},
\end{aligned} \tag{5}$$

where $\kappa = 2GM^2/\Delta_0$, $C_{\pm} = [(1 \pm 1/\sqrt{1+\kappa^2})/2]^{1/2}$, $C_{T,C} = (C_+ \pm C_-)/\sqrt{2}$, and $E_{I–IV}$ are listed with respect to $U(1)$. The parameter κ contains a squared 1D matrix element $M = |\langle \phi^+|x|\phi^-\rangle|^2$; it is easily obtained that $M \simeq 1 + 1/2\sqrt{\alpha\pi}$, where α is the ratio $\alpha = (\Delta x/a_0)^2 >> 1$, $a_0 = \sqrt{\hbar/m\omega_0}$ being the zero-point amplitude in the well of $U(x)$.

It follows from Eq. (5) that the coupling arranges the four zero-point levels symmetrically in two pairs, associated with *trans* and *cis* proton transfer localized along the x_s and x_a axis, respectively. This allows a simple estimate of the average energy and the tunneling splitting of the lowest pair of levels,

$$E_0 \equiv (E_{II} + E_I)/2 = \omega_0 - (1/2)\sqrt{\Delta_0^2 + 4G^2} - G,$$
$$\Delta E_0 \equiv E_{II} - E_I = \sqrt{\Delta_0^2 + 4G^2} - 2G. \tag{6}$$

It shows how the coupling reduces the 1D splitting if the two protons start to move as a pair. Equation (5) predicts that the same splitting with reversed sign applies to the next split pair of levels, but this is likely to be inaccurate because of the proximity of (neglected) excited levels. The dependence of the eigenvalues $E_{\mathrm{I–IV}}$ on G is shown in Fig. 3, where solid/open symbols correspond to +/− levels, with respect to ω_0 taken as origin.

Solution (5) represents the contribution of the lowest pair of states (ϕ_i^+, ϕ_i^-) of each particle $i = 1, 2$. Since ϕ_i^+ and ϕ_i^- are orthonormal, it thus represents an analogue in continuous variables of the four states of two coupled two-level systems (TLS_2); we will refer to it as a TLS_2-type solution. Its main feature is the two-proton entanglement represented by the antisymmetric functions Φ_{II}^- and Φ_{III}^-, which (in this approximation) are confined exclusively in the *trans* and *cis* configuration, respectively, independent of the coupling strength. Their symmetric counterparts Φ_{I}^+ and Φ_{IV}^+, respectively, contain contributions from both configurations, but with increasing coupling strength also tend to localize in the corresponding regions of the 2D space; this is seen from the behavior of the coefficients $C_{\mathrm{T,C}}$, which in the most typical regime, $\kappa >> 1$, take the form $C_{\mathrm{T}} \simeq 1 - 1/8\kappa^2; C_{\mathrm{C}} \simeq 1/2\kappa$. As we show in Subsection III C by explicit quantitative measures, this high degree of entanglement of the two protons in the ground state is entirely due to symmetry and therefore remains essentially unchanged in the exact solution. In Sec. IV we also show that it is of fundamental importance for the mechanism of co-tunneling of the two protons.

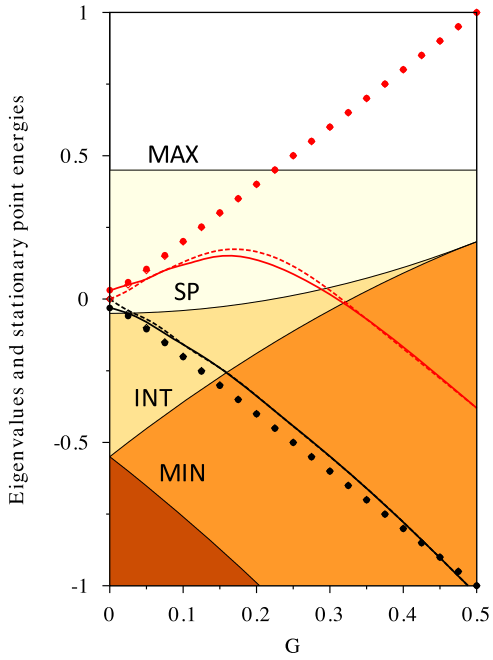

FIG. 3. Plot of the lowest four (dimensionless) eigenvalues of Hamiltonian (1,3) against the correlation factor G for $D = 0$. The remaining parameters are $U_0 = 1584\ \mathrm{cm}^{-1}$, $\Delta x = 0.34$ Å, and m = proton mass, which define the (dimensionless) parameters of 1D tunneling $\omega_0 = 0.550$, $\Delta_0 = 0.031$, and $g = 0.303$. Thick solid/broken lines depict the numerical eigenvalues referring to symmetric/antisymmetric levels of the 1st (black) and 2nd (red) pair; solid symbols depict the corresponding levels obtained from the analytical solution (5). Thin lines represent the stationary points of the potential as a function of G as indicated. Energies above MIN and below INT in orange, above INT and below SP in dark yellow and above SP and below MAX in light yellow.

B. The exact solution

The basis set that diagonalizes the 2D Hamiltonian is taken in the form of products of harmonic-oscillator wave functions, i.e., $\psi = \sum_{m,j} C_{m,j} \chi_m(x_1) \chi_j(x_2)$. Functions $\chi_m(x_1)$ and $\chi_j(x_2)$ are centered at $x_1 = x_2 = 0$ and chosen so that their zero-point amplitude equals the halfwidth Δx of the 1D potential. The secular equation then takes the form $\|H - E\|\psi = 0$, where the Hamiltonian matrix elements have the form

$$
\begin{aligned}
H_{m,n;j,k} &= H^0_{m,n;j,k} + V^{\mathrm{int}}_{m,n;j,k} \\
H^0_{m,n;j,k} &= h^{(\alpha)}_{m,n}\delta_{j,k} + h^{(\alpha)}_{j,k}\delta_{m,n}; \qquad V^{\mathrm{int}}_{\mathrm{m,n;j,k}} = -2Gx_{\mathrm{m,n}}x_{\mathrm{j,k}} - Dx^2_{m,n}x^2_{j,k} \\
h^{(\alpha)}_{p,q} &= [\alpha(2p+1) + (1/2)]\delta_{p,q} + (1/2)x^4_{m,n} - (1+\alpha)x^2_{m,n}; \quad \alpha = (1/2)g^2 \\
x^N_{j,k} &= \langle \chi_j(x)|x^N|\chi_k(x)\rangle.
\end{aligned}
\tag{7}
$$

Here $H^0_{m,n;j,k}$ represents the sum of the 1D Hamiltonian matrices $h^{(\alpha)}_{m,n}$ in Eq. (1); $V^{\mathrm{int}}_{m,n;j,k}$ represents the coupling term; $\delta_{p,q}$ are delta-symbols and $\langle \chi_j(x)|x^N|\chi_k(x)\rangle$ are harmonic-oscillator matrix elements. Because of the complexity of the 2D potential shown in Fig. 1(a), which has two sets of (inequivalent) minima, a large number of functions are required before convergence is achieved, but, due to the choice of the proper basis set, the resulting matrix is sparse enough to be amenable to a modified Jacobi-Davidson algorithm for sparse matrices.[8] The resulting eigenfunctions and eigenvalues (denoted by Roman numerals as in Sec. III A) are either symmetric, labeled by a superscript +, or antisymmetric, labeled by a superscript −, relative to the dividing plane of the proton motions. Symmetric states belong to the representation a_g and antisymmetric states to either the representation b_{3g} or b_{2u} depending on whether they are aligned along the *trans* or the *cis* axis, respectively. However, the order of the levels need not be the same as that in (5) but will depend on the model parameters, except for the ground level, E_{I}, which is always symmetric, while, for repulsive interaction ($G > 0$), the lowest pair of states is always aligned along the *trans* axis. The other pair of zero-point states, aligned along the *cis* axis, may or may not be next in the ladder

of states, depending on the parameter values, more specifically, on the energy of the first *trans* overtone.

In Fig. 3 we present a general picture of the dependence of the (dimensionless) lowest four eigenvalues on the strength of the dipole coupling in the range $0 \leq G \leq 0.5$ for $D = 0$, thus covering a full range of systems with secondary minima INT. The model parameters are typical for coupled hydrogen bonds (see caption of Fig. 3) and assign the first four states to the two pairs of zero-point states. The thick solid and broken lines display the eigenvalues for symmetric and antisymmetric levels, respectively, relative to an origin ω_0, which are to be compared with the eigenvalues of the four-level model of Subsection III A, namely, in the form of full symbols. The eigenvalues are plotted together with the energies of the stationary configurations, which also vary as a function of G; rescaled to ω_0, they assume the form $E_{\mathrm{MAX}} = 1 - \omega_0$, $E_{\mathrm{MIN}} = 1 - (1+G)^2 - \omega_0$, $E_{\mathrm{INT}} = 1 - (1-G)^2 - \omega_0$ and $E_{\mathrm{SP}} = \frac{1}{2} + G^2 - \omega_0$; in Fig. 3 they are depicted by thin lines. For zero G, the lowest four eigenvalues in Eq. (5) are exact; thus it follows directly from the model that for zero G, the lowest four eigenvalues, i.e., the zero-point levels, correspond to two symmetric eigenstates and a central degenerate antisymmetric eigenstate. Introduction of repulsive coupling splits the degenerate state into two antisymmetric components of different symmetry: b_{3g} for the lower and b_{2u} for the upper component. With increasing coupling, their separation increases rapidly. The two symmetric (a_g) levels also increase their separation, but more slowly, with the result that the lower pair separates from the upper pair forming a gradually closer doublet, while the upper two levels cross and reverse their ordering so as to become the same as that of the lower pair, i.e., symmetric below antisymmetric, which is the natural order for a pair of isolated tunneling levels. This behavior is superimposed on the general trend towards lower energies. This pattern can be readily understood on the basis of the corresponding changes in the potential and in the effective mass of the tunneling particle.

For the present model parameters, the lowest pair is located well above E_{INT} for coupling strengths up to $G \simeq 0.15$; hence the *cis* region of the 2D space is classically allowed for the lowest pair of eigenstates. However, the planar projections of the wave functions Φ_{I}^{+} and Φ_{II}^{-} in Fig. 4 show that this region is forbidden by symmetry, namely, strictly for the antisymmetric b_{3g} state but also, to an approximation depending on the coupling, for the symmetric state. This entanglement of the two protons represented by the exact eigenvectors is determined by symmetry, and as seen from this figure, bears close resemblance to that of the approximate solution (5). We quantify this entanglement in Subsection III C by introducing a new measure in continuous variables for the states of Hamiltonian (1,3).

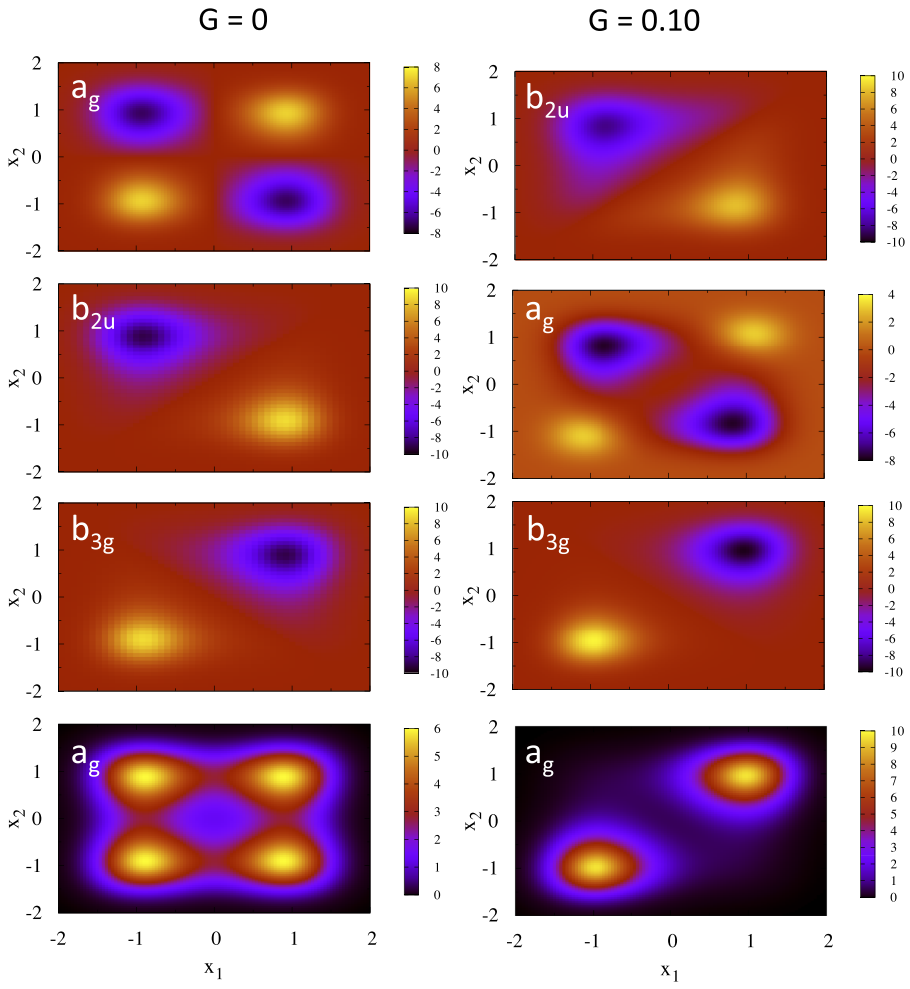

FIG. 4. Projections of the lowest four eigenfunctions of Hamiltonian (1,3) (from bottom to top), for $G = 0$ (left panels) and $G = 0.10$ (right panels); the remaining parameters are as in Fig. 3. The symmetry of the eigenfunctions is also indicated. The collective coordinates x_s and x_a in Eq. (2) are represented by the LL-RR and LR-RL diagonals, respectively.

C. Measure of entanglement in H_{2D}

The high degree of entanglement of the lowest states with increasing coupling manifests itself in strong localization along the collective coordinates x_s or x_a, i.e., along the LL-RR or LR-RL diagonal in Fig. 4, respectively. This localization means that the 2D wave functions lose their separability into products of individual-particle wave functions and become entangled,[24] as seen from a comparison of Φ_I^+ and Φ_{II}^- at $G = 0$, defined by Eq. (5) and illustrated in Fig. 4: $\Phi_I^+ = \phi_1^+\phi_2^+$ is separable, and thus not entangled, but exhibits equal "population" in all four "corners" LL, LR, RL, and RR of the 2D space $\{x_1, x_2\}$ in Fig. 4; $\Phi_{II}^- = (1/\sqrt{2})(\phi_1^+\phi_2^- + \phi_1^-\phi_2^+)$ is a Bell-type function (the 1D wave functions $\phi_i^{+,-}$ being orthonormal) and thus maximally entangled; it exhibits complete localization along x_s. This transformation is formalized by representing the solution (5) in terms of the localized basis set $\{\psi_{s,a}^T, \psi_{s,a}^C\}$, which forms a 2×2 analogue to the Bell functions expressed in continuous variables (CV). Indeed, recasting $\phi_i^{+,-}$ in the familiar form $\phi_i^{+,-} = (1/\sqrt{2})(|L>_i \pm |R>_i)$ via functions localized in the left/right well of $U(x_i)$, one obtains the standard Bell-type representation

$$\begin{aligned}\psi_{s,a}^T &= (1/\sqrt{2})(|LL> \pm |RR>);\\ \psi_{s,a}^C &= (1/\sqrt{2})(|LR> \pm |RL>).\end{aligned} \tag{8}$$

Accordingly, the eigenvectors (5) can be represented in a form analogous to that of TLS_2,

$$\Phi = \alpha|LL> + \beta|LR> + \gamma|RL> + \delta|RR>, \tag{9}$$

where the corresponding coefficients are defined in Eq. (5) via the parameter κ. For TLS_2, a common measure of entanglement is the Peres-Horodecki criterion,[25,26] which in the Wootters formulation[27] defines the concurrence measure

$$C = 2|\alpha\delta - \beta\gamma|. \tag{10}$$

To define which measure of entanglement in CV is adequate for H_{2D}, we recast this expression in a form applicable to the solution (5),

$$2|\alpha\delta - \beta\gamma| \equiv |P_s - P_a|, \tag{11}$$

where P_s and P_a are the probabilities of localization along the LL-RR and LR-RL diagonal, respectively,

$$P_s = \int_{x_1*x_2>0} |\Phi(x_1,x_2)|^2; \quad P_a = \int_{x_1*x_2<0} |\Phi(x_1,x_2)|^2. \tag{12}$$

Analogously, we formulate a general entanglement measure in CV, termed "confinement," for any (orthonormal) eigenstate $\Phi(x_1, x_2)$ of H_{2D} in the form

$$C_o = |P_s - P_a|. \tag{13}$$

For the approximate solution (5), the confinement measure is obtained analytically, the results being the same for the two pairs of states (Φ_I^+, Φ_{II}^-) and $(\Phi_{III}^-, \Phi_{IV}^+)$,

$$C_o^- \equiv C^- = 1; \quad C_o^+ \equiv C^+ = \kappa/\sqrt{1+\kappa^2}. \tag{14}$$

For the exact eigenstates obtained in Subsection III B, the confinement measure is obtained numerically; in Fig. 5, we illustrate its dependence on the coupling parameter G for the ground-state pair $\Phi_{I,II}$ of a system of which the other parameters are as in Figs. 3 and 4. Figure 5 quantifies the high degree of entanglement of these states in the most common regime $\kappa >> 1$, where $C_o^- \simeq 1$; $C_o^+ \simeq 1 - 1/2\kappa^2$.

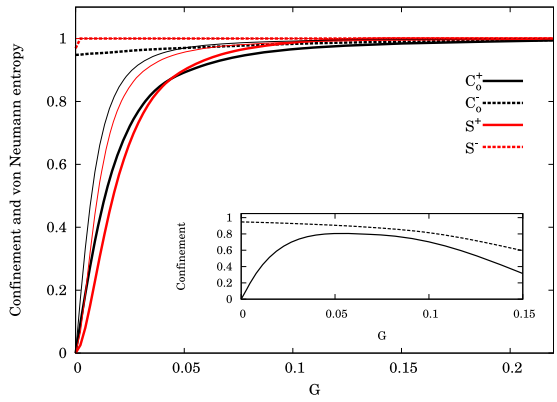

FIG. 5. Entanglement measures confinement $C_o^{+/-}$ (solid/dashed black curves) and von Neumann entropy $S^{+/-}$ (solid/dashed red curves) defined by Eqs. (13) and (16), respectively, for the lowest pair of states of Hamiltonian (1) as a function of the coupling strength G. Thin/thick lines represent the approximate/exact solutions, respectively. The inset represents $C_o^{+/-}$ for the 2nd pair of states. The remaining parameters are as in Fig. 3.

To illustrate the performance of the confinement measure, we compare it with the von Neumann entropy of the reduced state, which was shown to be a good entanglement measure in CV[28] and has been applied, e.g., to two-electron systems[29,30] as well as to the entanglement of electronic and vibrational degrees of freedom of a molecule.[31]

The eigenstates $\{\Phi(x_1, x_2)\}$ of Hamiltonian (1) are pure two-particle states. For a given eigenstate $|\Phi(x_1, x_2)\rangle$, the density matrix is $\hat{\rho} = |\Phi\rangle\langle\Phi|$ and the reduced density matrix is $\hat{\rho}^{red}(x_1, x_1') = \mathrm{tr}_2|\Phi(x_1, x_2)\rangle\langle\Phi(x_1', x_2)|$, where tr_2 indicates that the trace applies to x_2 only.[32,33] The von Neumann entropy of the reduced state, given by

$$S = -\mathrm{tr}(\hat{\rho}^{red}\log_2\hat{\rho}^{red}), \tag{15}$$

can be evaluated from the eigenvalues $\{\lambda\}$ of $\hat{\rho}^{red}$ in the form

$$S = -\sum_i \lambda_i \log_2 \lambda_i. \tag{16}$$

To find these eigenvalues, we use a basis set of N single-proton wave functions $\{\phi(x_i)\}$ of the type used in Sec. III A and first diagonalize the Hamiltonian, which yields the eigenfunctions in the form $\Phi(x_1, x_2) = \sum_{m,j=1}^N C_{m,j}\phi_m(x_1)\phi_j(x_2)$ (coefficients real). The reduced density matrix then is given by $\hat{\rho}^{red}(x_1, x_1') = \sum_{m,n=1}^N R_{m,n}\phi_m(x_1)\phi_n(x_1')$, where $R_{m,n} = \sum_{j=1}^N C_{m,j}C_{n,j}$. Its eigenvalues $\{\lambda\}$ are obtained by solving the secular problem $\|\hat{\rho}^{red} - \lambda\|\chi(x_1) = 0$, and for the approximate solution (5), which corresponds to $N = 2$, this can be done analytically; it yields again the same von Neumann entropy for the two pairs of states in the form

$$S^- = 1, \quad S^+ = -(C_+^2\log_2 C_+^2 + C_-^2\log_2 C_-^2), \tag{17}$$

so that $S^+ \simeq 1 - 1/\kappa^2 \ln 2$ at $\kappa >> 1$, similar to the confinement measure (14). For $N > 2$, the secular problem can only be solved numerically, and thus the eigenvalues $\{\lambda\}$ and hence S depend on N. We note that obtaining converging results for the von Neumann entropy turned out to be a non-trivial task since we deal with tunneling motions, whereby the eigenfunctions

$\Phi(x_1, x_2)$ are exponentially small in vast areas of the 2D space. In Fig. 5 we show the results for the ground-state pair $\Phi_{\rm I}^{+}$ and $\Phi_{\rm II}^{-}$ obtained with a basis set of $N = 46$ single-proton wave functions, which proved sufficient.

Figure 5 shows that, although not identical, the two entanglement measures $C_{\rm o}$ and S behave similarly, which proves the validity of the confinement as entanglement measure. It is physically transparent for the systems under consideration and much easier to calculate than the von Neumann entropy, once the 2D eigenfunctions are available. As illustrated by the figure, for meaningful parameter values, both criteria indicate a very high degree of entanglement of the ground-state pair, especially for the antisymmetric state. This is a consequence of the symmetry of the system, rather than of a specific behavior in the regime of "deep tunneling." In fact, for the parameters used, Fig. 5 illustrates that $C_{\rm o}^{+} > 0.95$ for couplings as low as $G \simeq 0.075$. It follows from Fig. 3 that in this parameter region, the ground-state pair of levels is well above the *cis* configuration INT (i.e., the LR-RL diagonal) so that the corresponding ground-state wave functions are classically allowed in this coordinate region. However, the strong entanglement confines these states almost exclusively to the *trans* configuration MIN (i.e., the LL-RR diagonal).

The same approach applies, in principle, to the second pair of zero-point states $\Phi_{\rm III}^{+}$ and $\Phi_{\rm IV}^{-}$, for which the *trans* region is symmetry forbidden there, but as Figs. 3 and 4 show, the effect of other states perturbs this simple pattern. While the coupling imposes *trans* localization on the b_{3g} state and *cis* localization on the b_{2u} state, the two a_g states can by symmetry spread over the entire plane. However, changing the coupling leads to mixing of the states since they have the same symmetry; this mixing will cause localization, as follows from the fact that stronger coupling leads to higher barriers and thus to more localized wave functions. On the other hand, stronger coupling also means stronger perturbation due to higher-energy states; as a result, the pattern of eigenvalues and of the entanglement of this pair of states is more complex, as shown in Figs. 3 and 5, respectively.

For the ground-state pair, the confinement of the symmetric state approaches that of the antisymmetric state for increasing coupling. Physically this corresponds to a proton pair that tunnels between two *trans* configurations. The mechanisms of these transitions, i.e., whether they move predominantly stepwise as single particles or concertedly as a double particle, are not immediately obvious. Now that we have shown how the eigenfunctions are governed by symmetry and how symmetry defines their entanglement, we can proceed with analyzing the mechanism; this problem is addressed in Sec. IV.

IV. MECHANISM OF CO-TUNNELING

A. The probability flux in the dividing surface

To quantify the mechanism of co-tunneling, we introduce a new tool based on the analysis of the probability flux within a pair of tunneling states. This flux, which is an integral over the dividing surface between two equivalent minima, is proportional to the tunneling splitting,[34] a relation known as the Herring formula.[35] In the presence of two tunneling particles, the distribution of the probability flux in the dividing plane contains all the information needed to study the mechanism of co-tunneling. We therefore propose to use this tool to determine the preferred mechanism of double-proton transfer in a given molecule or complex. In this section, we show how the quantum treatment can provide a quantitative measure for the degree of concertedness of two-particle tunneling and thus for the relative contributions of stepwise and concerted transfer mechanisms. We show also that these contributions are directly related to the entanglement of the particles, which is determined by symmetry.

For the present model Hamiltonian (3), the lowest pair of states is localized along the *trans-trans* path; the dividing plane thus is $x_{\rm s} = 0$ and the distribution of the probability flux is given by

$$F_{\rm s}(x_a) = \left[\Phi_{\rm I}^{+}(x_{\rm s}, x_{\rm a}) \frac{\partial \Phi_{\rm II}^{-}(x_{\rm a}, x_{\rm s})}{\partial x_{\rm s}}\right]_{x_{\rm s}=0}. \tag{18}$$

First we ensure the quality of the eigenfunctions by showing that the flux $\int_{-\infty}^{\infty} dx_{\rm a} F_{\rm s}(x_{\rm a})$ through the dividing plane is related to the zero-point splitting ΔE_0 obtained from the eigenvalues in accordance with the Herring formula,[35] which here takes the form

$$\Delta E_0 = \frac{1}{2} g_s^2 \frac{\int_{-\infty}^{\infty} dx_{\rm a} F_{\rm s}(x_{\rm a})}{\int_{-\infty}^{\infty} dx_{\rm a} \int_{0}^{\infty} dx_{\rm s} \Phi_{\rm I}^{+}(x_{\rm s}, x_{\rm a}) \Phi_{\rm II}^{-}(x_{\rm s}, x_{\rm a})}. \tag{19}$$

In terms of trajectories, this flux includes contributions from all possible transfer paths between the two MIN configurations. If $F_{\rm s}(x_{\rm a})$ peaks at $x_{\rm a} = 0$, the dominant path will be tunneling through MAX ($x_{\rm s} = x_{\rm a} = 0$); the transfer will then be concerted. If, on the other hand, the flux density peaks near $x_{\rm a} = \pm 1$, the dominant path will pass through INT $[x_{\rm s} = 0, x_{\rm a} = \pm\sqrt{(1-G)/(1-D)}]$; the transfer will then be stepwise. The question to what extent each of these mechanisms contributes to two-particle tunneling within a given pair of states can thus be answered by analyzing the flux distribution in the corresponding dividing plane. In Fig. 6(a) we plot such distributions for $G = 0$ and 0.10 for the same model parameters as used in Figs. 3 and 4. The plots are decomposed into the profiles of the wave function of the symmetric state $\Phi_{\rm I}^{+}(x_{\rm s}, x_{\rm a})_{x_{\rm s}=0}$ and the first derivative of the antisymmetric state $\left[\partial \Phi_{\rm II}^{-}(x_{\rm s}, x_{\rm a})/\partial x_{\rm s}\right]_{x_{\rm s}=0}$; the latter always peaks at $x_{\rm a} = 0$, where the antisymmetric wave function changes sign.

The most remarkable feature of this flux is its behavior at zero coupling $G = 0$. Then the lowest four eigenstates $\Phi_{\rm I-IV}(x_1, x_2)$ are given by the analytical solution (5), as combinations of products of the zero-point eigenfunctions $\phi^{\pm}$ of the two protons in the 1D potential $U(x)$. Since these can be approximated by ± combinations of harmonic-oscillator wave functions in the wells, it is easy to deduce the character of the projection of $\Phi_{\rm I}^{+}$ in the dividing plane $x_{\rm s} = 0$: it is represented by the sum of two overlapping Gaussians at $x_{\rm a} = \pm 1$, as one would expect for independent particles. However, because the eigenvector $\Phi_{\rm II}^{-}$ is antisymmetric, the derivative $|\partial \Phi_{\rm II}^{-}/\partial x_{\rm s}|_{x_{\rm s}=0}$ always has its maximum at $x_{\rm a} = 0$; as a result, the flux density acquires a value at the center that cannot be described in terms of two independent tunneling

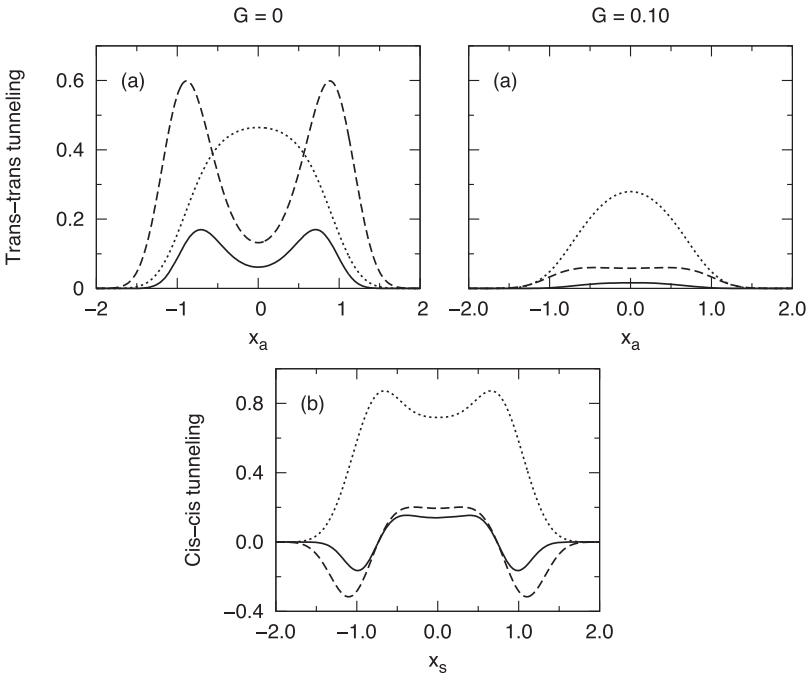

FIG. 6. Distribution of the probability flux in the dividing plane for the two pairs of zero-point states: (a) Distribution of $\Phi_{\rm I}^{+}$; $d\Phi_{\rm II}^{-}/dx_{\rm s}$ and the probability flux $F_{\rm s}(x_{\rm a})$ in the dividing plane $x_{\rm s}=0$ (*trans-trans* tunneling), depicted by solid, dot-dashed and dashed lines, respectively, for $G=0$ (left panel) and $G=0.10$ (right panel). The area under $F_{\rm s}(x_{\rm a})$ is proportional to the tunneling splitting obtained by diagonalization, as defined by Eq. (9). (b): Same as in (a) but for the 2nd pair $\Phi_{\rm III}^{+}$ and $\Phi_{\rm IV}^{-}$, in the dividing plane $x_{\rm s}=0$ (*cis-cis* tunneling; only for $G=0.10$). The remaining parameters are as in Fig. 3.

steps but reflects quantum-mechanical interference between stepwise and concerted tunneling. Although the two protons are not interacting, their wave functions remain entangled due to the equivalence of their configurations, as demonstrated in Sec. III C. Whatever the coupling, if there is symmetry, there will always be co-tunneling. This implies that the terms concerted and stepwise have only qualitative significance.

The degree of co-tunneling induced by coupling depends not only on G but also on the parameters g and D in Hamiltonian (1,3); for illustrative purposes, we set $D=0$, as in Fig. 3. An increase in G leads to increased confinement of the lowest pair of eigenstates along the *trans* axis, and thus increased entanglement, which will favor concertedness. As shown in Fig. 6(a), for the parameters of Fig. 3 and double-proton tunneling, concerted transfer becomes significant for a coupling as weak as $G=0.10$ since the flux peaks at $x_{\rm a}=0$, but is essentially "flat," with shoulders near $x_{\rm a}\simeq\pm0.5$, indicating stepwise transfer. The general dependence of the flux distribution on G in the range 0–0.22 is illustrated in Fig. 7 for the same parameters as above, which shows a gradual transition from two overlapping Gaussians for $G=0$ to a single peak for $G=0.22$, interpreted as the gradual replacement of stepwise by concerted transfer. Concurrently, the tunneling splitting decreases from single-proton-like to double-proton-like.

Similar plots can be produced for any set of model parameters (g, G, D). But it should be realized that a given molecule or complex is represented by a unique set of four model parameters, which together give a complete picture of the transfer mechanism. We return to this problem in Sec. V, where we deal with a realistic example.

These calculations show that, in the tunneling regime, both concerted and stepwise transfer occur under the conditions when the two mechanisms are competitive, i.e., the potential has two sets of minima. This conclusion is at variance with the conclusion, drawn from instanton analysis,[10] that for nonzero coupling the transfer is always concerted. It follows that the (conventional) one-instanton approach used in that earlier study, which associates the zero-point splitting with the concerted instanton $x_{\rm a}\equiv0$ at $T=0$ and ignores other instantons present in the case of two sets of minima, fails in this limit. However, the practical significance of this failure may be limited to systems with unusually weak couplings. For any given system, the question of the mechanism can be answered by calculating the probability flux and interpreting

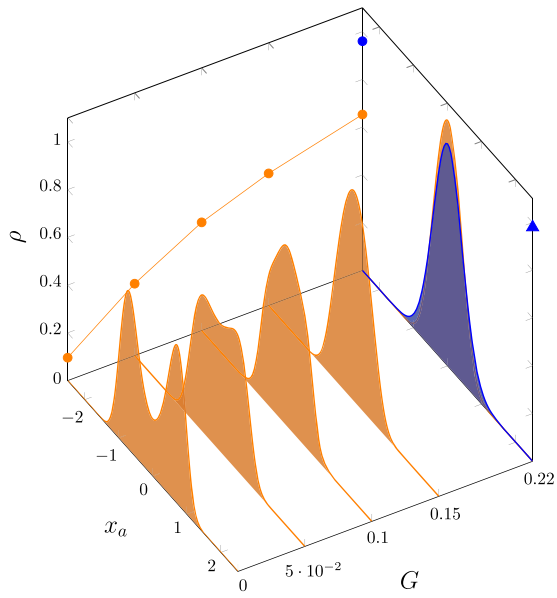

FIG. 7. Evolution of the flux distribution with the coupling strength G for zero-point (*trans-trans*) tunneling. The flux density is renormalized by the corresponding tunneling splitting so that the area under each curve equals unity. The vertical profiles (in orange) show the evolution of the flux distribution with G and the graph on the vertical panel illustrates the contribution of the concerted mechanism given by the ratio ρ in Eq. (21), for the same parameters as in Fig. 3. The blue color illustrates the flux distribution for porphycene treated in Sec. V, where $\rho\approx1$ (blue dot). The blue triangle indicates the confinement entanglement measure of the lowest pair of states of porphycene $C_{\rm o}^{+}\approx C_{\rm o}^{-}\approx1$.

the transfer as (predominantly) concerted if it shows a dominant central peak and (predominantly) stepwise if it shows twin peaks.

B. How much co-tunneling?

To obtain a quantitative measure of the contributions of each of these mechanisms to the zero-point splitting, we compare the 2D tunneling splitting ΔE_0, obtained from the diagonalization of the full Hamiltonian matrix (7), with its component for concerted tunneling, $\Delta E_{0,c}$, obtained by diagonalizing an effective 1D Hamiltonian for tunneling along x_s. The latter Hamiltonian, which we denote by $H^{1D}_{eff}(x_s)$, takes account of the zero-point energy of x_a; for the lowest pair of states $\Phi_{I,II}(x_1, x_2)$, it is obtained from Eq. (3) by replacing x_a^2 by its average value in the ground state $\langle x_a^2 \rangle = \langle \Phi_I(x_1, x_2)|x_a^2|\Phi_I(x_1, x_2)\rangle$,

$$H^{1D}_{eff}(x_s) = -\frac{1}{2}g_s^2\frac{\partial^2}{\partial x_s^2} + (1-D)\left[(x_s^2 - \Delta x_s^2)^2 + 2Rx_s^2\langle x_a^2\rangle\right]. \tag{20}$$

It is easily seen that the term proportional to R reduces the width (and height) of the 1D potential along x_s, thus leading to a larger splitting. By expressing the resulting splitting for the co-tunneling as the ratio

$$\rho = \Delta E_{0,c}/\Delta E_0, \tag{21}$$

we have thus obtained a quantitative measure for the contribution of the concerted mechanism to the tunneling splitting. In Table I we list ΔE_0, $\Delta E_{0,c}$, and ρ as functions of G in the range of $G \in (0, 0.5)$ for the model parameters used in Fig. 3. In Fig. 7 we show how the ratio ρ gradually increases with increasing coupling from 0.10 for vanishing coupling to 0.94 for the largest coupling compatible with the presence of two sets of minima. The Gaussian flux corresponding to concerted tunneling can be directly obtained from $\Delta E_{0,c}$ and compared with that obtained from diagonalization. For instance, for $G = 0.10$ illustrated in Fig. 6(a), the zero-point tunneling splitting obtained from the concerted path is $\Delta E_{0,c} = 2.9\ cm^{-1}$, which, compared with that obtained from diagonalization $\Delta E_0 = 6.4\ cm^{-1}$, implies that more than half of the flux is due to the alternative step-wise mechanism.

TABLE I. Zero-point tunneling splitting ΔE_0 and transfer mechanism as a function of G. ΔE_0 is obtained from direct diagonalization of Hamiltonian (1). The transfer mechanism is quantified by the ratio $\rho = \Delta E_{0,c}/\Delta E_0$, where $\Delta E_{0,c}$ is the splitting obtained from the 1D tunneling in Hamiltonian (20), which corresponds to concerted tunneling. The splittings are reported in cm^{-1}, which is the order-of-magnitude for double-proton transfer in coupled hydrogen bonds. Model parameters as in Fig. 3: $U_0 = 1584\ cm^{-1}$, $\Delta x = 0.34$ Å, $D = 0$, and m = proton mass.

G	ΔE_0	$\Delta E_{0,c}$	ρ
0	98.4	9.4	0.10
0.025	34.1	7.1	0.21
0.05	17.6	5.3	0.30
0.075	10.4	3.9	0.38
0.10	6.4	2.9	0.45
0.15	2.8	1.6	0.55
0.22	0.96	0.64	0.65
0.33	0.19	0.14	0.76
0.44	0.035	0.030	0.86
0.50	0.013	0.012	0.94

In principle, the method applied to the lower pair of zero-point levels can also be applied to the upper pair, where $x_a = 0$ is the dividing plane. The corresponding flux density for the *cis* tunneling takes the form

$$F_a(x_s) = \left[\Phi^+_{IV}(x_s, x_a)\frac{\partial \Phi^-_{III}(x_s, x_a)}{\partial x_a}\right]_{x_a=0}, \tag{22}$$

or, if the two levels have crossed, with interchanged subscripts III and IV (but no interchange of superscripts + and −). For zero coupling ($G = 0$), it is equivalent to the behavior of $F_s(x_a)$ in Fig. 6(a), with two peaks indicating stepwise transfer, but even for $G \geq 0.10$, its behavior is irregular with multiple peaks in its components, as illustrated in Fig. 6(b). This complex and strongly non-Gaussian shape implies interference from higher-energy states. It also confirms the well-known rule that the lowest pair of states is the most entangled.

V. APPLICATION TO PORPHYCENE

Porphycene is a molecule that is subject to double-proton transfer in a potential that represents two interchanging stationary isomers of symmetry C_{2h} and C_{2v}, which are both subgroups of the point group D_{2h}, representing a second-order saddle point, similar to MAX in our model Hamiltonian (1,3). To date it is the only molecule of this type for which a zero-point splitting has been measured, namely, that between the lowest two of the four zero-point levels in the electronic ground state.[36–38]

To model double-proton transfer of a given molecule or complex with N atoms, we formulate the $3N$-6 (vibrational) potential $\mathcal{V}$ in terms of the (mass-weighted) normal modes of the configuration of highest symmetry, which is the SP2 configuration; we denote these by $(X_s, X_a; Y)$, where $X_{s,a}$ denotes the two modes with imaginary frequencies and $\mathbf{Y}$ denotes the system of the remaining $3N - 8$ (skeletal) modes. We restrict $\mathcal{V}(X_s, X_a; \mathbf{Y})$ to terms harmonic in $\mathbf{Y}$ and quartic in X, and the $X\mathbf{Y}$ coupling to terms linear in $\mathbf{Y}$. For molecules of the point group D_{2h}, only modes that are displaced between the SP2 and the remaining stationary configurations are involved in this coupling, i.e., modes of symmetry a_g, b_{3g}, b_{1u}, and b_{2u}. This yields the multidimensional Hamiltonian in the presence of two tunneling coordinates in the following general form:

$$\mathcal{H} = -\frac{1}{2}\hbar^2\left(\frac{\partial^2}{\partial X_s^2} + \frac{\partial^2}{\partial X_a^2} + \frac{\partial^2}{\partial \mathbf{Y}^2}\right) + \mathcal{V}(X_s, X_a, \mathbf{Y}),$$

$$\begin{aligned}\mathcal{V}(X_s, X_a, \mathbf{Y}) = {} & \mathcal{V}_s(X_s) + \mathcal{V}_a(X_a) + 2RX_s^2X_a^2 \\ & + \frac{1}{2}\sum_{a_g}\omega^2\left(Y - \frac{C}{\omega^2}X_s^2 - \frac{C'}{\omega^2}X_a^2\right)^2 \\ & + \frac{1}{2}\sum_{b_{3g}}\omega^2\left(Y - \frac{C}{\omega^2}X_s\right)^2 + \frac{1}{2}\sum_{b_{2u}}\omega^2\left(Y - \frac{C}{\omega^2}X_a\right)^2 \\ & + \frac{1}{2}\sum_{b_{1u}}\omega^2\left(Y - \frac{C}{\omega^2}X_sX_a\right)^2. \end{aligned} \tag{23}$$

Here the frequencies of the skeletal modes are assumed constant and equal to their values ω at SP2. The profiles $\mathcal{V}_{s,a}(X_{s,a})$ along the tunneling coordinates are double-minimum potentials that we assume to be quartic: $\mathcal{V}(X) = -aX^2 + bX^4$, their corresponding barrier heights and widths, along with the coupling constant R, are directly found from the energies and positions of the stationary points. The coupling constants $\mathbf{C}$ of symmetry-allowed coupling terms $X\mathbf{Y}$ are found from the corresponding mode frequencies and displacements between the stationary points. All parameters of this Hamiltonian can thus be generated from the electronic structure and vibrational force-field calculations at the stationary configurations, as detailed elsewhere.[39]

As pointed out in the Introduction, the application of instanton techniques to a multidimensional Hamiltonian with two tunneling coordinates and two sets of (inequivalent) minima is complicated by interference problems. Full diagonalization is equally unfeasible at the present time, but since we are mainly concerned with the dynamics of the two protons, we will reduce the dimensionality by treating the skeletal modes collectively through approximations.

As a first step, we identify the two modes with imaginary frequency $X_{s,a}$ with the collective proton coordinates $x_{s,a}$ of Eqs. (2) and (3) through the relation $x_{s,a} = X_{s,a}/\sqrt{2m}\Delta x$, where m is the mass of an individual tunneling particle, i.e., proton or deuteron, etc. We thus neglect the small contributions of other atomic motions, which allows us to relate the calculated profiles along $X_{s,a}$ to the model profiles along $x_{s,a}$ in Eq. (3), as shown in the Appendix. The motion along $X_{s,a}$ is, however, subject to coupling to skeletal modes, the most important coupling terms being of the form $Y_{a_g}X_s^2$ and $Y_{b1u}X_sX_a$, where Y_{ag} and Y_{b1u} modes, are, respectively (predominantly), the + and − combination of the hydrogen-bridge modes of the two bonds and therefore the two modes most strongly coupled to the proton motion. However, they have an opposite effect on the collective tunneling of the two particles: the former shortens the two bonds symmetrically and will thus facilitate concerted transfer, while the latter breaks the symmetry of the two bonds and will thus facilitate stepwise transfer. Therefore special care must be exercised to choose approximations that are adequate for the hydrogen-bridge modes. As follows from Eq. (23), to treat these couplings properly, we would need a 4D effective Hamiltonian with two proton and two hydrogen-bridge coordinates. As this is not feasible at this time, we treat the two bridge modes collectively and, since they are "slow" relative to the proton motions, we choose the sudden approximation (SA), in which they are "frozen" during the tunneling; we use the same approximation for the remaining coupled skeletal modes, for all of which the coupling is weak. This approximation is justified for porphycene, as seen from the frequencies listed in Table II.

To implement this approach, the model of Eq. (1) first needs to be generalized so that it includes skeletal as well as proton motions. Applying the SA to the skeletal normal modes then leads to an effective 2D Hamiltonian for the proton coordinates of the form as in (1), with parameters renormalized so as to include the effect of these modes on the proton motion. A detailed account of this extension of the model will be given elsewhere;[20] in the Appendix we summarize the relations that define the renormalized model parameters through calculated quantities. All parameters involved are directly obtained from the calculated potential discussed above and are given by relations (A1)–(A8) of this Appendix. The resulting values for porphycene are collected in Table II. Using this set of parameters, we then diagonalize the effective 2D Hamiltonian (1); this yields the following eigenvalues for the lowest four states, listed in cm^{-1}: $E_{\mathrm{I}}^{+} = 2096$; $E_{\mathrm{II}}^{-} = 2104$; $E_{\mathrm{III}}^{+} = 3260$, and $E_{\mathrm{IV}}^{-} = 3491$, where the subscripts ± indicate the symmetry of the eigenstates.

TABLE II. Top part: Input parameters for the model Hamiltonian (1,3) for double-proton tunneling in porphycene, in the sudden approximation (SA) for the skeletal modes, adapted from the RI-CC2/cc-pVTZ calculations of Ref. 40: Δx in Å; G, D in dimensionless units; $\Delta X_{s,a}$ in Å $\mathrm{amu}^{1/2}$, all other parameters in cm^{-1}. Middle part: Energies of the stationary configurations, in cm^{-1}. Bottom part: Characteristic frequencies used to justify the SA: $\omega_{0,s/a}$ and $\omega^*_{s/a}$ are the calculated frequencies along the tunneling coordinates $X_{s,a}$ in the *trans* configuration and the SP2, respectively; $\omega_{a_g/b_{1u}}$ are the calculated frequencies of the hydrogen-bridge modes ate the SP2, in cm^{-1}.

Parameter	SA model	RI-CC2
U_0	1050	...
Δx	0.29	...
G	0.22	...
D	0.15	...
ω_0	1609	...
Δ_0	247	...
$\Delta X_{s/a}$	...	0.495/0.398
$\mathcal{E}_{r,s/a}$	2198/906	...
E_{MIN}	0	0
E_{INT}	2174	...
E_{SP}	2716	...
E_{MAX}	3837	...
$\omega_{0,s/a}$	...	2199/2716
$\omega^*_{s/a}$	...	i(1024/841)
ω_{a_g}/b_{1u}	...	275/350

As seen from Table II, the lowest pair of states is close to but below INT, i.e., they occupy the tunneling region of the complete 2D space. This is reflected in the properties of their wave functions, which have the typical character of a pair of states corresponding to *trans-trans* tunneling. The zero-point tunneling splitting of 7.9 cm^{-1} is reasonably close to the measured value of 4.4 cm^{-1}, although not as close as the value of 4.1 cm^{-1} obtained in the calculations of Ref. 30 with the *cis* tunneling coordinate frozen, due to the less accurate treatment of the skeletal modes.

On the other hand, the present 2D calculation provides information on the tunneling mechanism; as shown in Fig. 6, the probability flux distribution for the lowest pair of states shows a single peak, indicating that the transfer is concerted. Closer inspection shows that this flux is almost pure Gaussian, which is typical for concerted transfer and means that stepwise transfer makes no significant contribution (in this case $\rho = 0.98$). As seen from the general properties of Hamiltonian (1) discussed in Secs. II–IV, such a high level of concertedness implies strong proton entanglement. Indeed, the confinement measure (13) applied to the ground-state pair of states of porphycene Φ_{I}^{+} and Φ_{II}^{-} yields $C_{\mathrm{o}}^{+} = 0.97$; $C_{\mathrm{o}}^{-} = 0.99$, indicating that at low temperature the two protons are highly entangled.

Similar calculations apply also to the higher levels, but the results are not easily interpreted. The second pair of states is situated above both INT and SP of the potential, and only slightly below SP2, implying that the corresponding wave functions will be strongly delocalized. That this is indeed the case is seen from the large tunneling splitting of 231 cm^{-1}. Such large splittings cannot be detected by the methods used in Ref. 5 and indeed no other splitting is observed. The corresponding flux distribution in the plane $x_a = 0$ is similar to that in Fig. 6(b). It offers no obvious interpretation of the transfer mechanism.

Porphycene is a good example of how quantum mechanics and symmetry lead to counter-intuitive results: the second pair of states is located above both INT and SP, which means that the particles "face" only the central barrier at MAX, the entire "torus" around it being classically allowed. Nevertheless, the ± wave functions retain the character typical for *cis-cis* tunneling, with $x_a = 0$ as dividing plane, despite the position of the levels. Only much higher up the ladder of states this entanglement disappears, and the wave functions obtain the character of a "particle in a box."

VI. THE ONE-INSTANTON APPROXIMATION

In Ref. 40 we showed that for porphycene the tunneling splitting of the lowest *trans* level could be calculated with very good accuracy if the *cis* tunneling coordinate was frozen. The Gaussian form of the probability-flux distribution calculated in Sec. IV confirmed that the two protons move synchronously, i.e., as a single particle, which justifies to some extent the elimination of the second tunneling coordinate in that earlier study. It also justifies the use of the one-instanton approximation in Ref. 10, whereby the zero-point tunneling splitting was related to the 1D instanton connecting the global minima through the SP2, i.e., the concerted instanton of the present study. Since it is easier to apply than 2D diagonalization, it is useful to inquire under which conditions silencing of the secondary tunneling coordinate is a valid approximation. Clearly, these will be conditions that minimize interference between the different types of instantons possible in a potential with two sets of minima (INT and MIN). This is likely to be the case if these instantons are well separated energetically. A measure for this separation is the energy gap between INT and MIN; if this gap is of the order of a vibrational quantum, we may reasonably assume that, similar to the case of porphycene, the coupling parameter G is in the range where the lowest pair of states is strongly localized in the *trans* configuration, leading to a (predominantly) Gaussian flux distribution corresponding to concerted transfer. Whenever such a situation prevails, one can safely estimate the zero-point tunneling splitting by means of calculations for the concerted instanton.

Assuming such a situation, we evaluate below the zero-point tunneling splitting in this one-instanton approach. We start from the quasiclassical analogue of the 2D Hamiltonian, in the SA for the skeletal modes, formulated in terms of the real (mass-weighted) coordinates $X_{s,a}$,

$$\bar{H}(X_s, X_a) = \frac{1}{2}\dot{X}_s^2 + \frac{1}{2}\dot{X}_a^2 + \bar{\mathcal{V}}(X_s, X_a). \tag{24}$$

Here the potential is given by

$$\bar{\mathcal{V}}(X_s, X_a) = (\bar{\mathcal{V}}_{0,s}/\Delta X_s^4)(X_s^2 - \Delta X_s^2)^2 + (\bar{\mathcal{V}}_{0,a}/\Delta X_a^4)(X_a^2 - \Delta X_a^2)^2 + 2\bar{R}X_s^2X_a^2, \tag{25}$$

where $\Delta X_{s,a}$ are the (half)widths of the barrier along $X_{s,a}$; $\bar{\mathcal{V}}_{0,s}$ and $\bar{\mathcal{V}}_{0,a}$ are the corresponding barrier heights, and $\bar{\mathcal{R}}$ is the coupling constant, all renormalized in the SA.

In the one-instanton approximation, the zero-point tunneling splitting ΔE_0 for Hamiltonian (24) is given by the general expression[41]

$$\Delta E_0 = \mathcal{A}\exp(-S_E^0), \tag{26}$$

where S_E^0 is the Euclidean action at $T = 0$ (in units $\hbar$), i.e., the action in the upside-down potential formulated in imaginary time evaluated along the extremal trajectory (instanton),

$$S_E^0 = \int_{-\infty}^{\infty} d\tau\, \bar{H}[X_s(\tau), X_a(\tau)]. \tag{27}$$

The pre-exponential factor has the general form

$$\mathcal{A} = \sqrt{2S_E^0/\pi}\,\Gamma_l\Gamma_t, \tag{28}$$

where Γ_l is a "longitudinal" factor that depends on the shape of the potential along the instanton path and Γ_t is a "transverse" factor that reflects the effect of fluctuations of the instanton due to coordinates transverse to it.

The instanton trajectory at $T = 0$ satisfies the equations $\delta S_E/\delta X_s = 0$; $\delta S_E/\delta X_a = 0$, subject to the periodic conditions $X_s(\infty) = X_s(0)$, $X_a(\infty) = X_a(0)$. For 2D Hamiltonians of type (24) and (25), these equations always have a 1D solution $X_a \equiv 0$ corresponding to the concerted instanton, which at $T = 0$ is the path connecting the *trans* minima through the SP2.[10,15] The Euclidean action (27) then equals the 1D action for tunneling with energy $E = 0$ in the potential along the *trans* path,[42]

$$S_E^0 \equiv \int_{-\Delta X_s}^{\Delta X_s} dX_s \sqrt{2\bar{\mathcal{V}}(X_s)}; \quad \bar{\mathcal{V}}(X_s) = (\bar{\mathcal{V}}_{0,s}/\Delta X_s^4)(X_s^2 - \Delta X_s^2)^2, \tag{29}$$

which is easily found. The remaining quantity in Eq. (26) is the prefactor, of which the longitudinal component is known for potentials of quartic shape,[43] but there is no general cost-effective way to evaluate the transverse factor directly. Therefore, we had earlier[7–9] developed a method based on the adiabatic approximation to the transverse modes, which renormalizes the potential along the instanton to a potential that is vibrationally adiabatic (VA) over these modes. In the present case, the coordinate X_a plays the role of a transverse mode, and we evaluate the corresponding pre-factor Γ_t using the adiabatic approximation. It is justified if at the minimum of the potential, i.e., the *trans* configuration, the harmonic frequency $\omega_{0,a}$ along X_a is higher than its counterpart $\omega_{0,s}$ along X_s; this is the case for porphycene, as seen from Table II. The vibrationally adiabatic potential is taken in the same quartic form as in Eq. (29), but with a barrier height renormalized to $\bar{\mathcal{V}}_{0,s} - \frac{1}{2}\hbar\omega_{0,a}$. The final expression for the zero-point splittings ΔE_0 then takes the familiar form for a quartic potential,[43] namely,

$$\Delta E_0 = (\hbar\omega_{0,s}/\pi)\sqrt{24\pi S_E^0}\,\exp(-S_E^0); \quad S_E^0 = (4/3)\Delta X_s\sqrt{2(\bar{\mathcal{V}}_{0,s} - \hbar\omega_{0,a}/2)}. \tag{30}$$

The evaluation of the zero-point tunneling splitting associated with the concerted instanton for the 2D Hamiltonian (24) is thereby reduced to a 1D tunneling calculation. Since the result is in analytical form, it can always be used for an order-of-magnitude estimate before undertaking a 2D diagonalization.

We now apply this result to porphycene, using the relevant parameters from Table II. This yields $\Delta E_0 = 7.8$ cm^{-1}, in close agreement with the exact diagonalization result of Sec. V (7.9 cm^{-1}). Correspondingly, the distribution of the quasiclassical probability flux in the dividing plane $X_s = 0$ is indistinguishable from the quantum distribution. Hence for this molecule, the distribution of the probability flux as well as the zero-point tunneling splitting is accurately represented by the concerted instanton $X_a \equiv 0$ at $T = 0$. This is not a trivial result since in the presence of a second set of minima, multiple instantons are possible for the 2D Hamiltonian in Eq. (24) at $T = 0$, and the concerted instanton may or may not be stable. The fact that it describes the zero-point tunneling adequately is apparently due to the large energy gap between the two sets of minima in the potential. In porphycene this gap is two orders of magnitude larger than the *trans* tunneling splitting. This justifies the silencing of the *cis* tunneling coordinate for this molecule and thus shows that the accurate result for the zero-point splitting obtained in Ref. 40 is not due to a compensation of errors but is a consequence of the proper treatment of the coupling to skeletal modes. In this case, the multidimensional Hamiltonian corresponding to double-proton transfer turns into an imaginary-mode Hamiltonian for the remaining tunneling coordinate X_s and several of the skeletal modes coupled to it, but with a position-dependent mass of tunneling.[7–9,40] Hence these calculations remain very demanding computationally.

The question may arise whether the same conclusion holds for the splitting of the upper pair of zero-point levels. The answer is that it does not. Fig. 6(b) shows that the distribution of the probability flux between these levels does not resemble a Gaussian but has oscillatory behavior, implying interference effects from multiple instantons. Thus, in this case reduction to 1D concerted tunneling is not possible.

VII. CONCLUSION

We have addressed the question whether two protons, each moving between two equivalent minima, will move separately, i.e., stepwise or together, i.e., concerted. To deal with this question, which obviously depends on the degree of coupling between the protons, we have introduced a new general method for 2D proton tunneling, capable of providing a quantitative answer. It is based on numerical diagonalization of a 2D Hamiltonian, with the proton-transfer coordinates treated as reaction coordinates (imaginary normal modes), where the potential supports two sets of inequivalent minima. This diagonalization yields eigenvalues that can be compared with observed tunneling splittings and eigenfunctions that can be used to analyze the tunneling mechanism. For this analysis, we introduce a new method, based on the calculation of the probability flux between states and its distribution in the dividing plane. From this flux, the contribution of co-tunneling to the total transfer process can be deduced quantitatively.

The central result of the study is that co-tunneling is always present, and this is a consequence of quantum-mechanical interference due to symmetry restrictions. In fact, symmetry imposes entanglement of the protons even in the absence of formal coupling. In the presence of coupling, it forbids access to classically allowed regions even for totally symmetric states. The imposed localization results in the competition between tunneling mechanisms and in characteristic patterns of tunneling splitting. Based on this localization, we have introduced a new entanglement measure that shows that at low temperatures the two protons are highly entangled. This holds for a wide range of parameters of interest and can be shown to stem from a basic quality of the 2D Hamiltonian (1), namely, its isomorphism to that of a pair of two-level systems, such as qubits or spins, subject to Ising-type coupling. This isomorphism leads to many similarities in the properties of the two Hamiltonians, but also exhibits some oddities, which we report elsewhere.[20] These general considerations allow us to conclude that, for a wide range of parameters of interest, the lowest pair of states of Hamiltonian (1,3) represents a perfect example of highly entangled states in a system with continuous variables.

To demonstrate the validity of the method, we have applied it to porphycene, where the parameters of the model Hamiltonian are derived in an unambiguous manner from quantum-chemical calculations; specifically, the linearized coupling between the proton-transfer modes and the skeletal normal modes is included in the sudden approximation, which recognizes the fact that the most strongly coupled modes are essentially static during the proton tunneling. We have reproduced the observed tunneling splitting satisfactorily and identified the transfer mechanism as concerted. We have also shown that, under normal conditions, when they are in the ground state, the porphycene protons are highly entangled at low temperature, which may have interesting applications.

ACKNOWLEDGMENTS

Financial support from Ministerio de Economia y Competitividad of Spain (Research Grant No. CTQ2014-58617-R), the Consellería de Cultura, Educación e Ordenación Universitaria (Centro singular de investigación de Galicia acreditación 2016-2019, No. ED431G/09), and the European Regional Development Fund (ERDF) is gratefully acknowledged.

APPENDIX: RENORMALIZING THE 2D HAMILTONIAN

To renormalize the 2D Hamiltonian (1) so as to make it applicable to a specific system, we modify the four parameters by which it is determined, using the sudden approximation (SA) for the coupled skeletal normal modes $\mathbf{Y}$, taken to be harmonic. Here we summarize the relations that define the four modified parameters, to be identified by bar-over symbols; detailed derivations will be presented elsewhere.[20] In the SA, only the potential energy surface is renormalized. The modified barrier along X_s is given by

$$\bar{\mathcal{V}}_{0,s} = \mathcal{V}_{0,s} + \mathcal{E}_{r,s}; \quad \mathcal{E}_{r,s} = (1/2) \sum_{a_g, b_{3g}} (\omega_j \Delta Y_j)^2, \tag{A1}$$

where $\mathcal{V}_{0,s}$ is the corresponding barrier height of the vibrationally adiabatic (VA) potential (defined below), and $\mathcal{E}_{r,s}$ the total reorganization energy of the normal modes $\{Y_j\}$ of the SP2 configuration along the *trans* path (i.e., modes of a_g and b_{3g} symmetry). The same barrier height can be obtained through the model parameters, which thereby yields for the modified 1D barrier height

$$\bar{U}_0 = \bar{\mathcal{V}}_{0,s}/2(1-D)\Delta x_s^4. \tag{A2}$$

The remaining model parameters (Δx; G and D) are not affected by the SA.[20] To relate them to calculated quantities, we write the VA potential, which is obtained from the calculated potential (13) under the condition $\partial \mathcal{V}(X_s, X_a; \mathbf{Y})/\partial \mathbf{Y} = 0$; this yields

$$\mathcal{V}_{VA}(X_s, X_a) = \mathcal{V}_s(X_s) + \mathcal{V}_a(X_a) + 2RX_s^2X_a^2; \quad \mathcal{V}(X) = -aX^2 + bX^4, \tag{A3}$$

which is analogous to the model potential in Eq. (3), since we identify the collective tunneling coordinates $x_{s,a}$ in Eq. (2) with the modes with imaginary frequencies $X_{s,a}$ through the relations $x_{s,a} = X_{s,a}/\sqrt{2m}\Delta x$. The model potential (3) can be equated to this VA potential if the following condition is met: $\mathcal{V}_{0,s}/\Delta X_s^4 = \mathcal{V}_{0,a}/\Delta X_a^4$, where $(\mathcal{V}_{0,s}; \Delta X_s)$ and $(\mathcal{V}_{0,a}; \Delta X_a)$ are the height and width of the barriers along the *trans* and *cis* tunneling coordinates, respectively. Then the model parameters are directly obtained from these calculated positions and energies of the stationary points, which define the coupling constant $\mathcal{R}$,

$$\mathcal{R} = \left\{ \frac{\mathcal{V}_{0,s}\mathcal{V}_{0,a} \pm [\mathcal{V}_{0,s}\mathcal{V}_{0,a}\mathcal{V}_{SP}(\mathcal{V}_{0,a} + \mathcal{V}_{SP} - \mathcal{V}_{0,s})]^{1/2}}{\mathcal{V}_{0,s} - \mathcal{V}_{SP}} \right\} / \Delta X_s^2 \Delta X_a^2. \tag{A4}$$

The final relations that define the four model parameters ($\bar{U}_0$; Δx; G and D) through calculated quantities are summarized below: From the barrier widths, one readily obtains the dipole coupling

$$G = (\alpha - 1)/(\alpha + 1); \qquad \alpha = (\Delta X_s/\Delta X_a)^2. \tag{A5}$$

The parameter D of quadrupole coupling is obtained from Eq. (A4) through the relations,

$$D = (R-3)/(R+1); \qquad R = R\Delta X_s^2 \Delta X_a^2 / \sqrt{\mathcal{V}_{0,s}\mathcal{V}_{0,a}}. \tag{A6}$$

The width of the 1D barrier is then obtained from the relation,

$$\Delta x = \Delta X_s \sqrt{(1-D)/[2m(1+G)]}. \tag{A7}$$

From relations (A5) and (A6), one obtains the width Δx_s of the model potential in Eq. (3),

$$\Delta x_s = \sqrt{(1+G)/(1-D)}, \tag{A8}$$

which, substituted in Eq. (A2), along with the value of D from Eq. (A6), yields the last of the four parameters of the model, the renormalized 1D barrier height $\bar{U}_0$.

Relations (A1)–(A8) provide a closed calculation scheme to generate the model parameters in the SA through parameters of the calculated potential. All input parameters involved are obtained from electronic-structure and force-field calculations at the stationary configurations, as detailed in Ref. 39. The above scheme and relations were used to obtain the model parameters of porphycene in the SA, listed in Table II and applied in Sec. V.

[1] F. Brange, O. Malkoc, and P. Samuelsson, Phys. Rev. Lett. **114**, 176803 (2015).
[2] F. Madeja and M. Havenith, J. Chem. Phys. **117**, 7162 (2002).
[3] Z. Smedarchina, A. Fernández-Ramos, and W. Siebrand, Chem. Phys. Lett. **395**, 339 (2004).
[4] G. L. Barnes, S. M. Squires, and E. Sibert III, J. Phys. Chem. B **112**, 595 (2008).
[5] J. Waluk, Pure Appl. Chem. **88**, 1063 (2016).
[6] J. Waluk, Chem. Rev. **117**, 2447 (2017).
[7] A. Fernández-Ramos, Z. Smedarchina, and W. Siebrand, Phys. Rev. E **90**, 033306 (2014).
[8] Z. Smedarchina, W. Siebrand, and A. Fernández-Ramos, "Kinetics isotope effects in multiple proton transfer," in *Isotope Effects in Chemistry and Biology*, edited by A. Kohen and H.-H. Limbach (Taylor and Francis, New York, 2005), p. 521.
[9] Z. Smedarchina, W. Siebrand, and A. Fernández-Ramos, *Multiple Proton Transfer: From Stepwise to Concerted* (Wiley-VCH, Weinheim, Germany, 2007), Vol. 2, p. 895, and the original papers cited therein.
[10] Z. Smedarchina, W. Siebrand, and A. Fernández-Ramos, J. Chem. Phys. **127**, 174513 (2007).
[11] A. Accardi, I. Barth, O. Kühn, and J. Manz, J. Phys. Chem. A **114**, 11252 (2010).
[12] M. K. Abdel-Latif and O. Kühn, Chem. Phys. **368**, 76 (2010).
[13] M. K. Abdel-Latif and O. Kühn, Theor. Chem. Acc. **128**, 307 (2011).
[14] J. R. De la Vega, J. H. Busch, J. H. Schauble, K. L. Kunze, and B. E. Haggert, J. Am. Chem. Soc. **104**, 3295 (1982).
[15] V. A. Benderskii, S. Yu. Grebenshchikov, D. E. Makarov, and E. V. Vetoshkin, Chem. Phys. **185**, 101 (1994); V. A. Benderskii, S. Yu. Grebenshchikov, E. V. Vetoshkin, G. V. Mil'nikov, and D. E. Makarov, J. Phys. Chem. **98**, 3300 (1994); V. A. Benderskii, E. V. Vetoshkin, E. I. Kats, and H. P. Trommsdorff, Phys. Rev. E **67**, 026102 (2003).
[16] S. C. Creagh, J. Phys. A: Math. Gen. **27**, 4969 (1994).
[17] R. H. McKenzie, J. Chem. Phys. **141**, 104314 (2014).
[18] M. Bollhöfer and Y. Notay, Comput. Phys. Commun. **177**, 951 (2007).
[19] Z. Smedarchina, M. F. Shibl, O. Kühn, and A. Fernández-Ramos, Chem. Phys. Lett. **436**, 314 (2007).
[20] Z. Smedarchina, W. Siebrand, and A. Fernández-Ramos (unpublished results).
[21] X.-G. Wang, T. Carrington, Jr., R. Dawes, and A. W. Jasper, J. Mol. Spectrosc. **268**, 53 (2011).
[22] T. Hammer and U. Manthe, J. Chem. Phys. **136**, 054105 (2012).
[23] W. Siebrand, Z. Smedarchina, and A. Fernández-Ramos, J. Chem. Phys. **139**, 021101 (2013).
[24] R. Horodecki, P. Horodecki, M. Horodecki, and K. Horodecki, Rev. Mod. Phys. **81**, 865 (2009).
[25] A. Peres, Phys. Rev. Lett. **77**, 1413 (1996).
[26] M. Horodecki, P. Horodecki, and R. Horodecki, Phys. Lett. A **223**, 1 (1996).
[27] W. K. Wootters, Phys. Rev. Lett. **80**, 2245 (1998).
[28] G. C. Ghirardi and L. Marinatto, Phys. Rev. A **70**, 012109 (2004).
[29] A. Ferrón, O. Osenda, and P. Serra, Phys. Rev. A **79**, 032509 (2009).
[30] O. Osenda and P. Serra, Phys. Rev. A **75**, 042331 (2007).
[31] L. K. McKemmish, R. H. McKenzie, N. S. Hush, and J. R. Reimers, J. Chem. Phys. **135**, 244110 (2011).
[32] E. R. Davidson, *Reduced Density Matrices in Quantum Chemistry* (Academic, New York, 1976).
[33] H. Nakatsuji, in *Many-Electron Densities and Reduced Density Matrices*, edited by J. Cioslowski (Kluwer Academic, New York, 2000).
[34] A. Jain and E. L. Sibert III, J. Chem. Phys. **142**, 084115 (2015).
[35] C. Herring, Rev. Mod. Phys. **34**, 631 (1962).
[36] J. Sepioł, A. Stepanenko, A. Vdovin, A. Mordzinski, E. Vogel, and J. Waluk, Chem. Phys. Lett. **296**, 549 (1998).
[37] J. Waluk, Acc. Chem. Res. **39**, 945 (2006).

[38]A. Vdovin, J. Waluk, B. Dick, and A. Slenczka, ChemPhysChem **10**, 761 (2009).
[39]See, e.g., Z. Smedarchina, W. Siebrand, and A. Fernández-Ramos, J. Chem. Phys. **137**, 224105 (2012), Appendix, and the original papers cited therein.
[40]Z. Smedarchina, W. Siebrand, and A. Fernández-Ramos, J. Chem. Phys. **141**, 174312 (2014).
[41]S. Coleman, in *The Whys of Subnuclear Physics*, edited by A. Zichichi (Plenum, New York, 1979), p. 805; A. I. Vainshtein, V. I. Zakharov, V. A. Novikov, and M. A. Shifman, "ABC of instantons," Sov. Phys. Usp. **25**, 195(1982); V. A. Benderskii, D. E. Makarov, and C. H. Wight, Adv. Chem. Phys. **88**, 1 (1994).
[42]J. P. Sethna, Phys. Rev. B **24**, 698 (1981).
[43]H. Dekker, Phys. Lett. A **114**, 295 (1985).